Structure and Chemical Bonding of PrRuSn

Jan F. Riecken[a], Adel F. Al Alam[b], Bernard Chevalier[b], Samir F. Matar[b], and Rainer Pöttgen[a]

[a] Institut für Anorganische und Analytische Chemie, Universität Münster, Corrensstraße 30, D-48149 Münster, Germany
[b] CNRS, Université de Bordeaux, ICMCB, 87 Avenue du Docteur Albert Schweitzer, F-33608 Pessac Cedex, France

Reprint requests to R. Pöttgen. E-mail: pottgen@uni-muenster.de

Z. Naturforsch. **2008**, *63b,* 1062 – 1068; received June 3, 2008

The new ternary stannide PrRuSn was synthesized from the elements *via* arc-melting. PrRuSn is isopointal to the orthorhombic TiNiSi-type structure, space group *Pnma*. The structure was characterized by X-ray powder and single crystal diffraction: $a = 761.7(2)$, $b = 483.9(2)$ and $c = 730.3(3)$ pm, $wR2 = 0.0386$, 433 F^2 values, 20 variables. The ruthenium and tin atoms in PrRuSn build up a three-dimensional [RuSn] polyanionic network with Ru–Sn distances in the range 268 – 274 pm. The praseodymium atoms fill channels within the polyanion. They bind to the network *via* short Pr–Ru distances of 301 and 302 pm. Electronic structure calculations on PrRuSn and isopointal PrPdSn underline these features and reveal strong *T*–Sn (*T* = Ru, Pd) interactions within both solid state structures.

Key words: Intermetallics, Stannide, Crystal Chemistry, Chemical Bonding

Introduction

Among the large family of rare earth (*RE*)-transition metal (*T*)-stannides [1], those with ruthenium as *T* component have only scarcely been investigated. The early rare earth elements form the stannides $RERuSn_3$ (*RE* = La–Nd) [2, 3] which crystallize in a site occupancy variant of the $Yb_3Rh_4Sn_{13}$ type [4]. Many tin-rich rare earth ruthenium stannides have been synthesized [5 – 8] when searching for new superconducting materials with structures related to $Tb_5Rh_6Sn_{18}$ [9, 10]. Furthermore, a whole series of $RERu_4Sn_6$ (*RE* = Y, La, Ce, Pr, Nd, Sm, Gd) stannides [11 – 15] with the tetragonal YRu_4Sn_6-type structure [11] has been reported. Especially $CeRu_4Sn_6$ has intensively been studied with respect to its low-temperature properties (heavy-fermion behavior, quantum fluctuations) [12 – 14, 16 – 19].

Recently we synthesized CeRuSn [20], the first equiatomic compound in the *RE*-Ru-Sn systems. Besides Ce_2RuZn_4 [21], CeRuSn is one of the rare examples of intermediate-valent cerium compounds with trivalent/intermediate-valent cerium ordering on distinct crystallographic sites. At r. t., CeRuSn adopts a superstructure of the monoclinic CeCoAl type [22] by doubling the subcell *c* axis. Susceptibility measurements [20] and electronic structure calculations [23] have fully underlined the trivalent/intermediate-valent cerium ordering of this outstanding stannide. During our phase analytical investigations of the neighboring *RE*-Ru-Sn systems we recently obtained the new stannide PrRuSn with a TiNiSi [24] related structure. The synthesis, crystal chemistry and chemical bonding of this stannide are reported herein.

Experimental Section

Synthesis

Starting materials for the synthesis of PrRuSn were an ingot of praseodymium metal (Johnson-Matthey), ruthenium powder (Degussa-Hüls, *ca.* 200 mesh), and tin granules (Merck), all with stated purities better than 99.9 %. Pieces of the praseodymium ingot were first arc-melted [25] to a small button under an argon atmosphere. The argon was purified before with molecular sieves, silica gel, and titanium sponge (900 K). Subsequently the praseodymium button, ruthenium powder and pieces of the tin granules were arc-melted. The sample was remelted three times to ensure homogeneity. The polycrystalline sample is stable in air over weeks.

EDX data

Semiquantitative EDX analyses of the crystal investigated on the diffractometer were carried out with a Leica 420i scan-

Table 1. Crystal data and structure refinement for PrRuSn, space group *Pnma*, $Z = 4$.

Empirical formula	PrRuSn
Formula weight, g mol^{-1}	360.67
Crystal size, μm^3	$20 \times 40 \times 60$
Unit cell dimensions a, pm	761.7(2)
b, pm	483.9(2)
c, pm	730.3(3)
V, nm^3	0.2692(2)
Calculated density, g cm^{-3}	8.90
Transm. ratio (max/min)	1.77
Absorption coefficient, mm^{-1}	32.2
$F(000)$, e	612
θ range data collection, deg	3 – 30
Range in hkl	$-10 \rightarrow +9$; ± 6; ± 10
Total no. reflections	2705
Independent reflections	433
R_{int}	0.079
Reflections with $I \geq 2\sigma(I)$	367
R_{sigma}	0.038
Data / parameters	433 / 20
Goodness-of-fit on F^2	1.051
$R1/wR2$ [$I \geq 2\sigma(I)$]	0.021 / 0.037
$R1/wR2$ (all data)	0.030 / 0.039
Extinction coefficient	0.0016(2)
Largest diff. peak / hole, e Å^{-3}	1.85 / −1.27

ning electron microscope with PrF_3, Ru, and Sn as standards. The experimentally observed composition (31 ± 3 at.-% Pr: 34 ± 3 at.-% Ru: 35 ± 3 at.-% Sn) was close to the equiatomic one. No impurity elements heavier than sodium (detection limit of the instrument) were found.

X-Ray diffraction

The polycrystalline sample was characterized through X-ray powder diffraction (Guinier technique, imaging plate detector, Fujifilm BAS-1800) using Cu$K_{\alpha 1}$ radiation and α-quartz (a = 491.30, c = 540.46 pm) as an internal standard. The orthorhombic lattice parameters (Table 1) were refined from the powder data by a least-squares routine. The proper indexing was ensured by an intensity calculation [26].

Table 3. Interatomic distances (pm) in PrRuSn, calculated with the powder lattice parameters. Standard deviations are all equal or smaller than 0.2 pm. All distances within the first coordination spheres are listed. The interatomic distances of PrPdSn [40] are listed for comparison.

PrRuSn				**PrPdSn**			
Pr:	1	Ru	301.2	Pr:	1	Pd	311.7
	1	Ru	301.7		2	Pd	317.1
	2	Ru	318.8		2	Sn	324.6
	2	Sn	324.3		2	Sn	332.4
	2	Sn	330.3		1	Sn	332.7
	1	Sn	334.0		1	Sn	337.9
	1	Sn	336.7		2	Pd	342.9
	2	Pr	370.3		1	Pd	349.5
	2	Ru	389.1		2	Pr	380.1
	2	Pr	391.0		2	Pr	397.4
Ru:	1	Sn	267.6	Pd:	1	Sn	268.5
	1	Sn	268.6		2	Sn	273.1
	2	Sn	273.6		1	Sn	289.8
	1	Pr	301.2		1	Pr	311.7
	1	Pr	301.7		2	Pr	317.1
	2	Pr	318.8		2	Pr	342.9
	2	Ru	343.8		1	Pr	349.5
	2	Pr	389.1		2	Pd	406.5
Sn:	1	Ru	267.6	Sn:	1	Pd	268.5
	1	Ru	268.6		2	Pd	273.1
	2	Ru	273.6		1	Pd	289.8
	2	Pr	324.3		2	Pr	324.6
	2	Pr	330.3		2	Pr	332.4
	1	Pr	334.0		1	Pr	332.7
	1	Pr	336.7		1	Pr	337.9

Small single crystals of PrRuSn were selected from the crushed sample, and their quality was checked by Laue photographs on a Buerger camera using white Mo radiation. Intensity data were collected at r.t. by use of a four-circle diffractometer (CAD4) with graphite-monochromatized MoK_α radiation and a scintillation counter with pulse height discrimination. The scans were taken in the $\omega/2\theta$ mode, and an empirical absorption correction was applied on the basis of ψ-scan data, accompanied by a spherical absorption correction. All relevant details concerning the data collection and evaluation are listed in Table 1.

Table 2. Atomic coordinates and anisotropic displacement parameters (pm^2) for PrRuSn. U_{eq} is defined as one third of the trace of the orthogonalized U_{ij} tensor. The anisotropic displacement factor exponent takes the form: $-2\pi^2[(ha^*)^2U_{11} + \ldots + 2hka^*b^*U_{12}]$. $U_{12} = U_{23} = 0$. The atomic positions of PrPdSn (neutron powder diffraction data from [40]: a = 744.5(2), b = 465.97(15) and c = 795.4(2) pm) are listed for comparison.

Atom	Wyckoff position	x	y	z	U_{11}	U_{22}	U_{33}	U_{13}	U_{eq}
PrRuSn:									
Pr	4c	0.96988(7)	1/4	0.68933(6)	64(2)	59(2)	66(2)	−7(2)	63(1)
Ru	4c	0.15109(9)	1/4	0.05586(8)	71(4)	62(3)	66(3)	−2(2)	66(2)
Sn	4c	0.30396(8)	1/4	0.38734(7)	52(3)	49(2)	76(2)	−8(2)	59(1)
PrPdSn:									
Pr	4c	0.0181	1/4	0.7017					
Pd	4c	0.2979	1/4	0.4102					
Sn	4c	0.1871	1/4	0.0889					

Structure refinement

The structural relationship of PrRuSn with the orthorhombic TiNiSi type [24] was already evident from the Guinier pattern. Accordingly, space group *Pnma* was found to be the correct one. The starting atomic parameters were then deduced from an automatic interpretation of a Direct Methods solution [27]. The setting was then transformed to the standard setting used for all previous structure refinements [28 – 30, and refs. cited therein]. Subsequently the structure was refined using SHELXL-97 [31] (full-matrix least-squares on F^2) with anisotropic atomic displacement parameters for all atoms. As a check for possible mixed occupied sites, all occupancy parameters were refined in separate series of least-squares cycles. Since all sites were fully occupied within two standard deviations, the ideal occupancies were assumed again in the final cycles. The final difference Fourier synthesis was flat (Table 1). The positional parameters and interatomic distances are listed in Tables 2 and 3.

Further details of the crystal structure investigation may be obtained from Fachinformationszentrum Karlsruhe, 76344 Eggenstein-Leopoldshafen, Germany (fax: +49-7247-808-666; e-mail: crysdata@fiz-karlsruhe.de, http://www.fiz-informationsdienste.de/en/DB/icsd/depot.anforderung.html) on quoting the deposition number CSD-419477.

Computational details

The electronic structure calculations for PrRuSn and PrPdSn were performed using the augmented spherical wave (ASW) method [32, 33] built within the density functional theory (DFT) framework [34, 35]. All valence states were treated as band states. In the minimal ASW basis set, the outermost shells were chosen to represent the valence states using partial waves up to $l_{max}+1=4$ for Pr, and $l_{max}+1=3$ for the transition metal and for Sn. The completeness of the valence basis set was checked for charge convergence, *i. e.* less than 0.1 electrons for $l_{max}+1$. The self-consistent field calculations were run to a convergence of 10^{-8} for the charge density. The accuracy of the method is in the range of about 10^{-8} Ryd. (1 Ryd. = 13.6 eV) regarding energy differences. The effects of exchange and correlation were treated based on the local density approximation LDA [36]. With three f electrons for Pr, the $4f$ subshell is only partially filled. From this, the single particle scheme of the LDA or GGA is good enough, as we could recently show for the stannide CeRuSn [23]. This calls for the introduction of a Coulomb on-site repulsion parameter within extra LDA+U/GGA+U-based calculations. Such preliminary calculations were carried out to check this point. They showed only a small departure from the single-particle picture, *e. g.* the lowering of the $4f$ density of states (DOS) at the Fermi level, pushing it down in energy.

First, spin-degenerate, non-magnetic (NM) calculations were carried out for the analysis of chemical bonding, then spin-polarized (SP) calculations were done to check for a possible onset of ordered magnetic moments on the constituent species. We note here that an NM configuration does not correspond to the paramagnetic one which could be achieved for instance by using supercells with random spin orientations.

In electronic structure calculations the interactions between atoms can be examined by the crystal orbital overlap population (COOP) introduced by Hoffmann [37] in Extended Hückel-type calculations and later on implemented within the ASW code [38]. In short-hand notation avoiding extended equations, the COOP can be looked at as the DOS weighted by the overlap integral S_{ij} between two chemical species i and j, carrying the same unit as the DOS of inverse energy (eV^{-1}). In the plots, positive, negative and zero magnitudes of COOP are indicative of bonding, antibonding, and nonbonding interactions, respectively.

Discussion

Crystal chemistry

Besides intermediate-valent CeRuSn [20, 23], PrRuSn is the second equiatomic stannide in the *RE*RuSn series. While CeRuSn crystallizes with its own peculiar monoclinic structure type, a TiNiSi-related structure occurs for PrRuSn. A comparison of the lattice parameters of PrRuSn (a = 761.7(2), b = 483.9(2), c = 730.3(3) pm) with those of the closely related structure of PrPdSn (a = 744.5(2), b = 465.97(15), c = 795.4(2) pm) [39, 40] already indicated a different structural distortion in PrRuSn. Calculation of the ratios a to c and $(a+c)$ to b for both stannides readily showed that these two compounds lie at different positions in the structure-field diagram of $PbCl_2$-related compounds [41]. For a detailed discussion of this geometrical model we refer to an overview by Jeitschko and Altmeyer [41].

These different structural distortions strongly influence the coordination of the praseodymium atoms as emphasized in Fig. 1. Both structures can be considered as orthorhombically distorted, ordered superstructures of the well known aristotype AlB_2. Overviews on the crystal chemistry, the group-subgroup relations and chemical bonding within this huge family of compounds are given in recent review articles [42 – 47]. Formation of the TiNiSi-related structure for the *RET*Sn stannides seems to depend on the electron count, because PrRhSn [48] crystal-

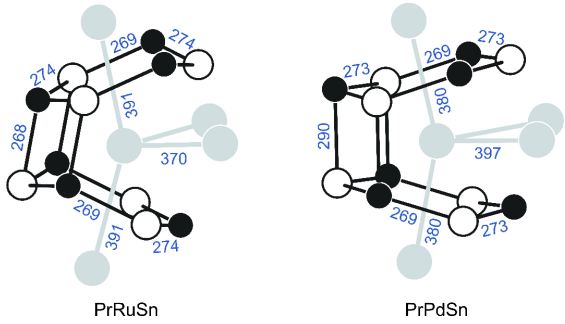

Fig. 1. Coordination of the praseodymium atoms in PrRuSn and PrPdSn [40]. The praseodymium, ruthenium (palladium), and tin atoms are drawn as light grey, black filled, and open circles, respectively. Relevant interatomic distances are indicated. For details see text.

lizes in the hexagonal ZrNiAl-type structure. Given the different distortions, and thus different bonding patterns in PrRuSn and PrPdSn, these structures are rather isopointal than isotypic [49, 50].

Together, the ruthenium (palladium) and tin atoms build up three-dimensional [RuSn] and [PdSn] networks in the PrRuSn and PrPdSn structures with Ru–Sn and Pd–Sn distances ranging from 268 – 274 and 269 – 290 pm, respectively (Table 3). These distances are close to the sums of the covalent radii of 264 pm (Ru + Sn) and 268 pm (Pd + Sn) [51], indicating significant Ru–Sn and Pd–Sn bonding. This is further shown in the chemical bonding analysis below. For PrRuSn, the Ru–Sn distances are similar to those in CeRuSn (265 – 290 pm) [20].

The [RuSn] and [PdSn] networks in PrRuSn and PrPdSn are built up from differently tilted Ru_3Sn_3 and Pd_3Sn_3 hexagons (Fig. 1). These hexagons are much more tilted in PrRuSn as compared to PrPdSn. This causes longer Pr–Pr distances (391 pm) along the *a* axis. Since the coordination polyhedron is then somewhat open on one side, the other two praseodymium neighbors move towards the central praseodymium atoms leaving shorter Pr–Pr contacts at 370 pm. The inverse behavior occurs for PrPdSn. The more planar hexagons move towards each other, and consequently the Pr–Pr distances along the *a* axis become smaller (380 pm), while the other two praseodymium neighbors move away from the central praseodymium atom and keep longer (397 pm) Pr–Pr distances. This distortion pattern is similar to the structures of the germanides CeRhGe and CeIrGe ([52] and refs. therein). The Pr–Pr distances in both stannides are slightly longer than the average Pr–Pr distance of 367 pm in hexagonal praseodymium with an *ABAC* stacking sequence [53].

The different tilts of the hexagons directly influence the distances of the praseodymium atom from its nearest neighbor atoms. In both stannides, PrRuSn and PrPdSn, the transition metal atoms have the closest contacts, however, with significantly shorter distances for the former. Similar to the CeRuSn structure [20] we observe short Pr–Ru distances (301 and 302 pm) also in PrRuSn (Table 3). These are only slightly longer than the sum of the covalent radii of 289 pm [51], and we can assume significant Pr–Ru bonding as it is further shown in the following computational section. In PrPdSn, the two shortest Pr–Pd distances of 312 and 317 pm are longer.

Finally, we need to comment on the differently tilted Ru_2Sn_2 and Pd_2Sn_2 parallelograms within the polyanionic networks (Fig. 1). As outlined in detail by Nuspl *et al.* [43], these tilts are a consequence of the electronegativity differences of the elements building the polyanionic network. The more electronegative component always occupies the position with the maximum distance in order to minimize the repulsion. Concerning the structures of PrRuSn and PrPdSn, the transition metals play a different role. In PrRuSn, the higher charge density is accumulated at the tin atoms, leading to closer Ru–Ru contacts of 344 pm within the parallelograms. The latter, however, are longer than in *hcp* ruthenium (6×270 and 6×265 pm [53]). In contrast, the more electronegative palladium atoms show the maximum separation in PrPdSn (407 pm). This peculiar pattern of chemical bonding is addressed explicitly in the following paragraph.

Electronic structure and chemical bonding analyses

At self-consistent convergence little charge transfer was observed between the atoms. In intermetallic systems it can be rather argued that the quantum mixing between the different valence states of the constituents is the underlying mechanism of bonding as it will be explicated first from the site-projected density of states (PDOS) and from an analysis of the chemical bonding based on overlap populations.

In Fig. 2, showing the site-projected density of states (PDOS) for PrRuSn and PrPdSn, the Fermi level (E_F) is taken as zero energy. This is also done in the following plots describing the chemical bonding. A major feature of a large DOS at E_F, $n(E_F)$, is observed in both

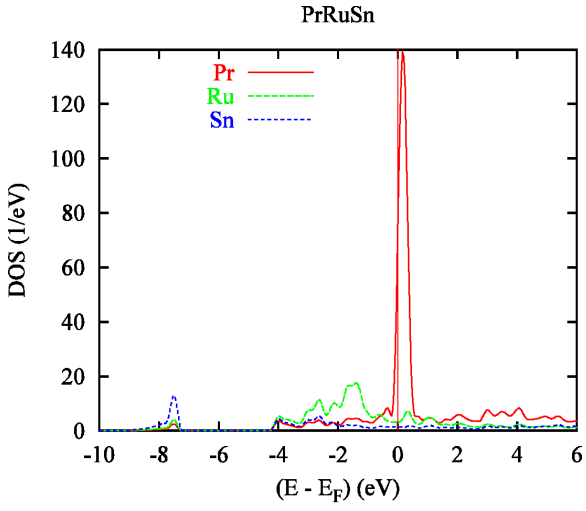

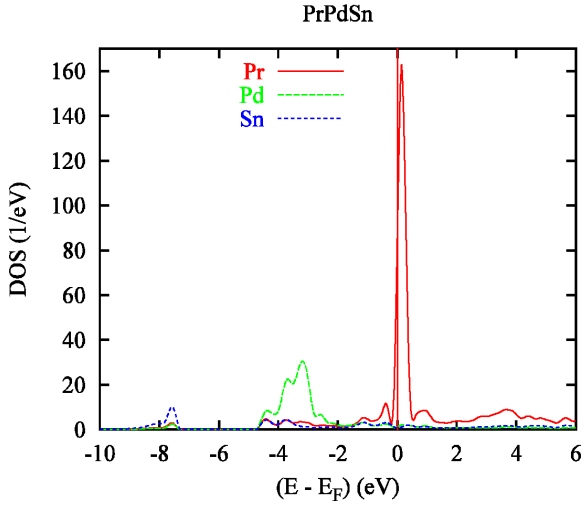

Fig. 2 (color online). Site-projected density of states (PDOS) of PrRuSn (top) and PrPdSn (bottom).

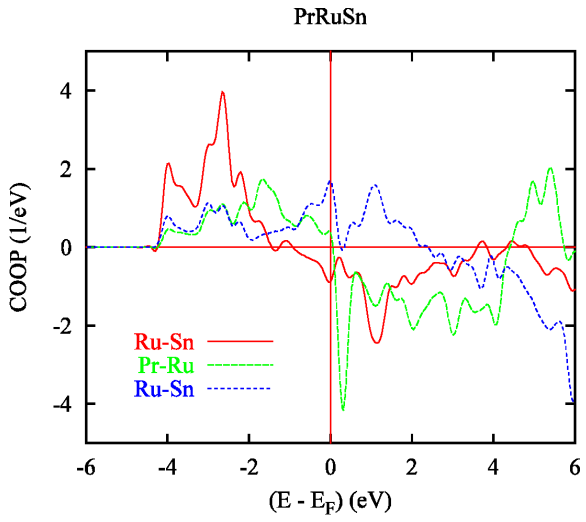

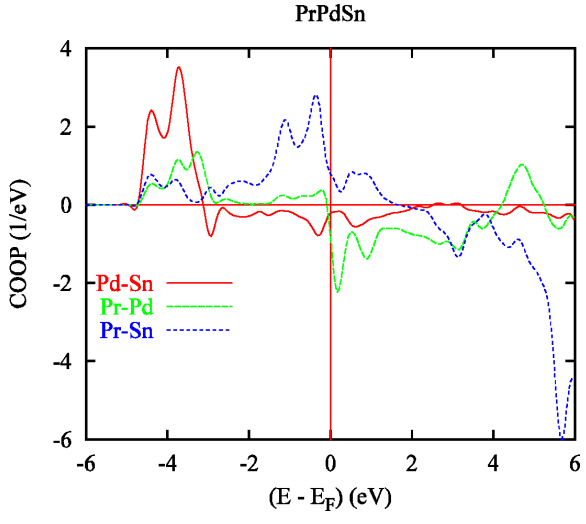

Fig. 3 (color online). Chemical bonding of PrRuSn (top) and PrPdSn (bottom) from the COOP criterion. Positive, negative, and zero COOP are relevant to bonding, antibonding, and non-bonding interactions, respectively.

systems for the Pr ($4f$) states whose major part lies, as one expects from their low filling, above E_F. In the mean-field Stoner theory of band ferromagnetism [54], this is indicative of instability of the system in such an NM configuration. Further, due to the larger filling of $4d$ states of Pd ($4d^8$) with 2 more electrons than Ru ($4d^6$) the former are centered at ~ -4 eV below E_F while the $4d$ states of ruthenium are only at ~ -2 eV below E_F. In these energy regions most of the quantum mixing between the different consituents, Pr (itinerant part), T (Ru, Pd) and Sn, is seen to occur. However, a better analysis of such mixing will be explained in the next paragraph describing the chemical bonding. In the lower part of the valence band (VB), around -8 eV, s-like states of tin are mainly found; they show a skyline similar to the less intense Pr and T PDOS.

Spin-polarized (SP) calculations were carried out for the stannide PrRuSn. Such calculations were preliminary in the sense that no extensive analyses of magnetic cells *versus* the nuclear cell were attempted. The calculations show that Pr carries a magnetic moment of 2.1 μ_B, but Ru a moment of ~ -0.15 μ_B. Being a

4*d* element albeit isolelectric with 3*d* Fe, Ru is not expected to carry a proper moment. Its low magnitude and the negative sign point to an induced nature of this moment. This is expected from the closeness of Ru (4*d*) states to Pr (4*f*) states on one hand and to the *f*-*d* overlap between Pr and Ru on the other hand. Magnetic and neutron powder diffraction experiments are planned to clarify this behavior.

The chemical bonding as analyzed through the overlap population with the COOP criterion is illustrated in Fig. 3 for PrRuSn and PrPdSn, respectively. The plots give details of the different interactions atom-to-atom between Pr, *T* and Sn. The major part of the VB is found to bear a bonding character for these interactions; the antibonding counterpart is found above E_F, in the conduction band. The strongest bonding peak intensity is observed between *T* and Sn. For the Ru–Sn interaction the COOP peak extends over the energy window [−4 to −2 eV] while it is narrower and centered at lower energy over the energy window [−5 to −3 eV] for PrPdSn. This follows from the lower lying Pd (4*d*) states with respect to the more extended Ru (4*d*) states at higher energy *versus* E_F and Pr (4*f*). This is mirrored by the Pr–Ru interaction which is found larger than Pr–Pd, hence the induced moment on Ru by Pr when SP calculations were performed.

Pr–Sn bonding is observed to be larger in the Pd compound than in the Ru one, especially near the top of the VB. While the average Pr–Sn distance of ∼ 330 pm, which is similar in both systems, cannot explain this feature, the difference in magnitude is likely to be due to the mixing of Pr states with both Ru and Sn states in PrRuSn, while only Sn states are mixing with Pr in the energy window −2 eV up to E_F. Further, within this energy interval, filling of $4d^8$(Pd) states with two more electrons with respect to the $4d^6$(Ru) states occurs. This suggests stronger Pr–Sn bonding within PrPdSn.

Acknowledgements

This work was financially supported by the Deutsche Forschungsgemeinschaft. B. C. and R. P. are indebted to EGIDE and DAAD for research grants within the PROCOPE program (11457RD and D/0502176). Finally, B. C. thanks the European Science Foundation (ECOMCOST action P16) for financial support. Computational facilities provided by the University of Bordeaux, Pole M3PEC-Mésocentre Aquitain, are gratefully acknowledged.

[1] R. V. Skolozdra in *Stannides of the rare-earth and transition metals*, (Eds.: K. A. Gschneidner Jr., L. Eyring), *Handbook on the Physics and Chemistry of Rare Earths*, Vol. 24, Elsevier, Amsterdam **1997**, chapter 164.
[2] B. Eisenmann, H. Schäfer, *J. Less-Common Met*. **1986**, *123*, 89.
[3] T. Fukuhara, I. Sakamoto, H. Sato, *J. Phys.: Cond. Matter* **1991**, *3*, 8917.
[4] J. L. Hodeau, J. Chenavas, M. Marezio, J. P. Remeika, *Solid State Commun*. **1980**, *36*, 839.
[5] G. P. Espinosa, *Mater. Res. Bull*. **1980**, *15*, 791.
[6] A. S. Cooper, *Mater. Res. Bull*. **1980**, *15*, 799.
[7] G. P. Espinosa, A. S. Cooper, H. Barz, J. P. Remeika, *Mater. Res. Bull*. **1980**, *15*, 1635.
[8] G. P. Espinosa, A. S. Cooper, H. Barz, *Mater. Res. Bull*. **1982**, *17*, 963.
[9] D. M. Vandenberg, *Mater. Res. Bull*. **1980**, *15*, 835.
[10] S. Miraglia, J. L. Hodeau, F. de Bergevin, M. Marezio, *Acta Crystallogr*. **1987**, *B43*, 76.
[11] G. Venturini, B. Chafik El Idrissi, J. F. Marêché, B. Malaman, *Mater. Res. Bull*. **1990**, *25*, 1541.
[12] I. Das, E. V. Sampathkumaran, *Phys. Rev. B* **1992**, *46*, 4250.
[13] I. Das, E. V. Sampathkumaran, *Phys. Rev. B* **1995**, *51*, 1308.
[14] R. Pöttgen, R.-D. Hoffmann, E. V. Sampathkumaran, I. Das, B. D. Mosel, R. Müllmann, *J. Solid State Chem*. **1997**, *134*, 326.
[15] M. F. Zumdick, R. Pöttgen, *Z. Naturforsch*. **1999**, *54b*, 863.
[16] E. M. Brüning, M. Baenitz, A. A. Grippius, A. M. Strydom, F. Steglich, R. E. Walstedt, *J. Magn. Magn. Mater*. **2007**, *310*, 393.
[17] A. M. Strydom, A. D. Hillier, D. T. Adroja, S. Paschen, F. Steglich, *J. Magn. Magn. Mater*. **2007**, *310*, 377.
[18] E. M. Brüning, M. Baenitz, A. A. Grippius, S. Paschen, A. M. Strydom, F. Steglich, *Physica B* **2006**, *378 – 380*, 839.
[19] A. M. Strydom, Z. Guo, S. Paschen, R. Viennois, F. Steglich, *Physica B* **2005**, *359 – 361*, 293.
[20] J. F. Riecken, W. Hermes, B. Chevalier, R.-D. Hoffmann, F. M. Schappacher, R. Pöttgen, *Z. Anorg. Allg. Chem*. **2007**, *633*, 1094.
[21] R. Mishra, W. Hermes, U. C. Rodewald, R.-D. Hoffmann, R. Pöttgen, *Z. Anorg. Allg. Chem*. **2008**, *634*, 470.
[22] O. M. Sichevich, V. A. Bruskov, R. M. Rykhal', Y. P. Yarmolyuk, *Sov. Phys. Crystallogr*. **1983**, *28*, 346.
[23] S. F. Matar, J. F. Riecken, B. Chevalier, R. Pöttgen, A. F. Al Alam, V. Eyert, *Phys. Rev. B* **2007**, *76*, 174434.

[24] C. B. Shoemaker, D. P. Shoemaker, *Acta Crystallogr.* **1965**, *18*, 900.
[25] R. Pöttgen, T. Gulden, A. Simon, *GIT Labor-Fachzeitschrift* **1999**, *43*, 133.
[26] K. Yvon, W. Jeitschko, E. Parthé, *J. Appl. Crystallogr.* **1977**, *10*, 73.
[27] G. M. Sheldrick, SHELXS-97, *Program for the Solution of Crystal Structures*, University of Göttingen, Göttingen (Germany) **1997**.
[28] J. F. Riecken, G. Heymann, T. Soltner, R.-D. Hoffmann, H. Huppertz, D. Johrendt, R. Pöttgen, *Z. Naturforsch.* **2005**, *60b*, 821.
[29] B. Chevalier, R. Decourt, B. Heying, F. M. Schappacher, U. Ch. Rodewald, R.-D. Hoffmann, R. Pöttgen, R. Eger, A. Simon, *Chem. Mater.* **2007**, *19*, 28.
[30] J. F. Riecken, G. Heymann, H. Huppertz, R. Pöttgen, *Z. Anorg. Allg. Chem.* **2007**, *633*, 869.
[31] G. M. Sheldrick, SHELXL-97, *Program for Crystal Structure Refinement*, University of Göttingen, Göttingen (Germany) **1997**.
[32] A. R. Williams, J. Kübler, C. D. Gelatt, *Phys. Rev. B* **1979**, *19*, 6094.
[33] V. Eyert, *The Augmented Spherical Wave Method – A Comprehensive Treatment*, Lect. Notes Phys. 719, Springer, Berlin **2007**.
[34] P. Hohenberg, W. Kohn, *Phys. Rev. B* **1964**, *136*, 864.
[35] W. Kohn, L. J. Sham, *Phys. Rev. A* **1965**, *140*, 1133.
[36] S. H. Vosko, L. Wilk, M. Nusair, *Can. J. Phys.* **1980**, *58*, 1200.
[37] R. Hoffmann, *Angew. Chem. Int. Ed. Engl.* **1987**, *26*, 846; *Angew. Chem.* **1987**, *99*, 871.
[38] V. Eyert, S. F. Matar, unpublished results.
[39] D. T. Adroja, S. K. Malik, *Phys. Rev. B* **1992**, *45*, 779.
[40] M. Kolenda, S. Baran, A. Olés, N. Stüsser, A. Sytuła, *J. Alloys Compd.* **1998**, *269*, 25.
[41] W. Jeitschko, R. O. Altmeyer, *Z. Naturforsch.* **1990**, *45b*, 947.
[42] E. Parthé, L. Gelato, B. Chabot, M. Penzo, K. Cenzual, R. Gladyshevskii, TYPIX–*Standardized Data and Crystal Chemical Characterization of Inorganic Structure Types. Gmelin Handbook of Inorganic and Organometallic Chemistry*, 8th edition, Springer, Berlin **1993**.
[43] G. Nuspl, K. Polborn, J. Evers, G. A. Landrum, R. Hoffmann, *Inorg. Chem.* **1996**, *35*, 6922.
[44] G. A. Landrum, R. Hoffmann, J. Evers, H. Boysen, *Inorg. Chem.* **1998**, *37*, 5754.
[45] R. Pöttgen, *Z. Kristallogr.* **2001**, *216*, 127.
[46] M. D. Bojin, R. Hoffmann, *Helv. Chim. Acta* **2003**, *86*, 1653.
[47] M. D. Bojin, R. Hoffmann, *Helv. Chim. Acta* **2003**, *86*, 1683.
[48] R. Mishra, R. Pöttgen, R.-D. Hoffmann, H. Trill, B. D. Mosel, H. Piotrowski, M. F. Zumdick, *Z. Naturforsch.* **2001**, *56b*, 589.
[49] L. M. Gelato, E. Parthé, *J. Appl. Crystallogr.* **1987**, *20*, 139.
[50] E. Parthé, L. M. Gelato, *Acta Crystallogr.* **1984**, *A40*, 169.
[51] J. Emsley, *The Elements*, Oxford University Press, Oxford **1999**.
[52] S. F. Matar, E. Gaudin, B. Chevalier, R. Pöttgen, *Solid State Sci.* **2007**, *9*, 274.
[53] J. Donohue, *The Structures of the Elements*, Wiley, New York **1974**.
[54] L. Kübler, V. Eyert, in *Electronic and Magnetic Properties of Metals and Ceramics, Electronic Structure Calculations*, Volume Part I, (Ed. K. H. J. Buschow), *Materials Science and Technology – A Comprehensive Treatment*, Vol. 3A, VCH, Weinheim **1992**, pp. 1 – 145.